Further considerations on the structure and bonding in edge-sharing bioctahedral complexes

Rinaldo Poli*,† and Raymund C. Torralba

Department of Chemistry and Biochemistry, University of Maryland, College Park, MD 20742 (USA)

(Received January 26, 1993; revised May 26, 1993)

Abstract

Extended Huckel MO calculations have been carried out on model compounds that mimic transition metal edge-sharing bioctahedral (ESBO) complexes of stoichiometry $M_2X_6L_4$ (X = anionic ligand with lone pairs for bridge-bonding and for π bonding, L = neutral 2-electron donor ligand), and for the corresponding mononuclear *cis*-MX_4L_2 system. The widening of the *cis*-L_{eq}–M–L_{eq} angle (eq = equatorial) is shown to cause the narrowing of the opposite X–M–X angle which, for the ESBO complexes, disfavors the formation of a strong metal–metal interaction. The calculations also address the importance of the M–X π interactions in metal–metal bonded dimers. The X_{ax} (ax = axial) ligands are shown to be better π donors than the X_{eq} ligands for the configurations d^1–d^1 through d^5–d^5, the differential between the π donating abilities in the two different positions being maximal for the d^1–d^1 configuration. This effect is proposed to be responsible for the preference of d^1–d^1 systems for the ESBO structure having all L ligands in equatorial positions, whereas the metal–metal bonded ESBO compounds of all other electronic configurations as well as all non-bonded ESBO complexes prefer the structure with two L_{eq} on one metal and two L_{ax} on the other one on steric grounds. The MO model presented here is also in excellent agreement with the observed trends of M–Cl_{ax}, M–Cl_{eq} and M–Cl_{br} (br = bridging) bond distances as a function of d^n–d^n configuration.

Introduction

For decades now, numerous compounds having the structure of an edge-sharing bioctahedron (ESBO) have been prepared. A few years ago, the structure and bonding of these and other M_2L_{10} systems was investigated by Hoffmann and co-workers [1]. A particular class of ESBO compounds that has received considerable attention is that corresponding to the stoichiometry $M_2X_6L_4$, where X is a negatively charge ligand with available lone pairs for bridge-bonding and/or for π donation and L is a 2-electron neutral donor. Derivatives of this class that have been characterized crystallographically have a central metallic core consisting of Zr_2^{6+} and Hf_2^{6+} (d^1–d^1) [2], Nb_2^{8+} and Ta_2^{8+} (d^1–d^1) [3], Nb_2^{6+} and Ta_2^{6+} (d^2–d^2) [4], Cr_2^{6+} (d^3–d^3) [5], Mo_2^{6+} (d^3–d^3) [6], MoW^{6+} (d^3–d^3) [7], W_2^{6+} (d^3–d^3) [8], Re_2^{6+} (d^4–d^4) and Re_2^{7+} (d^3–d^4) [9], Ru_2^{6+} (d^5–d^5) [10], and Rh_2^{6+} (d^6–d^6) [11]. These compounds are of interest from several different perspectives, including metal–metal bonding and magnetic interactions, stereoisomerism, and stereoselectivity in reactions. Structural aspects of this class of ESBO compounds, with the focus on the metal–metal interaction, have been reviewed by Cotton [12]. In compounds of this class, the bridging positions are always occupied by X ligands. The distribution of the remaining X and L ligands in the eight terminal positions can lead, in principle, to numerous stereoisomers, but typically only the ones with higher symmetry, shown in **I**–**IV**, are found to exist.

Our interest in this field has been fueled by the discovery in our laboratory that minor changes in the nature of phosphine substituents have a profound effect on the M–M interaction in ESBO $Mo_2Cl_6L_4$ (L = monodentate tertiary phosphine). For $L = PEt_3$, the two molybdenum centers are 3.730(1) Å apart [6e], indicating the absence of a metal–metal bond. On the other hand, for $L = PMe_2Ph$, the Mo–Mo distance is only 2.8036(8) Å and the compound is substantially diamagnetic [6f], consistent with the existence of a direct Mo–Mo bond and the pairing of the six available metal electrons in a $\sigma^2\pi^2\delta^{*2}$ ground state configuration [6f]. Both compounds exist solely, both in the solid state and in solution, as type **II** isomers. By the use of paramagnetic ^1H NMR, we have established that the ability of the

*Author to whom correspondence should be addressed.

†Presidential Young Investigator 1990–1995, Alfred P. Sloan Research Fellow 1992–1994.

two metal centers to bind to each other increases continuously along the series of $Mo_2Cl_6(PMe_xEt_{3-x})_4$ ($x=0$, 1, 2, 3) complexes from $x=0$ (no Mo–Mo bond and weak antiferromagnetic coupling) to $x=3$ (strong Mo–Mo bond, substantially diamagnetic) [6g]. We have also established that the metal–metal bonding interaction decreases dramatically on going from the $Mo_2Cl_6(PMe_2Ph)_4$ compound to its hexabromide analogue [13]. We argued that differences in the σ-donating abilities of the phosphines could not account for this tremendous effect, because the better σ-donor PEt_3 ligand would be predicted to facilitate the formation of the metal–metal bond through a more effective expansion of the metal orbitals, whereas experimentally, among the hexachloride derivatives, the compound with PEt_3 is the only one found to completely lack a bonding interaction [6f, g]. The question therefore arose as to whether steric effects could be responsible for this phenomenon, since PEt_3 has a cone angle 10° greater than PMe_2Ph, and 14° greater than PMe_3 [14].

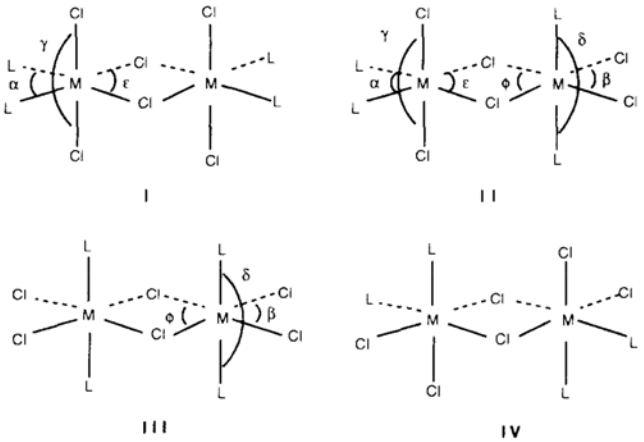

I II III IV

Previous attention to the importance of steric effects in ESBO complexes has been primarily focused on the *syn*–ax,ax interaction (A in diagram **V**) [1]. For instance, the failure of $Re_2Cl_6(dppe)_2$ (dppe = 1,2-bis(diphenylphosphino)ethane), of type **I** [9a], to show a metal–metal bonding interaction has been attributed [1] to the destabilizing type A interaction between the axial chlorine lone pairs (this rationalization has been later revisited) [6f, 12, 15]. Structure **III** is usually adopted only by complexes where the two *syn*–axial ligands are tied together by a backbone, typically a single methylene group such as in the family of diphosphine ligands $R_2PCH_2PR_2$. This is again attributed to the unfavorable type A steric interaction which would occur between two monodentate L ligands in a type **III** structure. Little attention has been given to another possible source of steric destabilization, that is, B in diagram **V**. It was suggested to us by a reviewer of our previous contribution on the type **II** $Mo_2Cl_6(PMe_xEt_{3-x})_4$ complexes [6g] that the opening of the P_{eq}–Mo–P_{eq} angle as a result of the increase in the bulk of the phosphine may cause the opposite angle (Cl_{br}–Mo–Cl_{br}) to close, hence forcing the metals to move apart and destabilizing the metal–metal bond. This effect has been pictorially described by the reviewer as 'reverse scissoring effect', a terminology that we would like to adopt. This observation has prompted theoretical investigations on our part, the results of which are reported here.

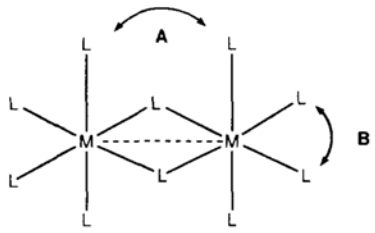

V

Another aspect of the ESBO structures that has puzzled us and others is the observation that $M_2X_6L_4$ complexes with a d^1–d^1 electronic configuration, whether the L ligands are monodentate or part of a bidentate unit, invariably show a structure of type **I** [2, 3], whereas those with more than one valence d electron on each metal, i.e. d^2–d^2 to d^6–d^6, always show a structure of type **II** when the ligands are monodentate [4a, i, 5, 6e, f, 8a, c, d, e, 10a, 11a]. Type **I** and **III** structure have been observed for the d^2–d^2 to d^6–d^6 dimers only when chelating ligands are present [4b–h, 5, 6a–d, 7, 8b, 9, 11b]. Structure **IV** is seldom observed for complexes of transition metals and still in conjunction with chelating ligands [6a, 9c]. It is also important to remark that in all known d^1–d^1 complexes the metals are bonded to each other. In complexes with electronic configurations d^3–d^3 to d^5–d^5, whereas metal–metal bonding is usually observed, a few non-bonded examples have been reported, e.g. $Cr_2Cl_6(PEt_3)_4$ [5], $Mo_2Cl_6(PEt_3)_4$ [6e] and $Ru_2Cl_6(PBu_3)_4$ [10a]. There are, to the best of our knowledge, no known examples of ESBO complexes for the electronic configuration d^0–d^0, where a metal–metal bonding interaction cannot of course exist. For d^6–d^6 complexes, a metal–metal bond cannot be established because there are as many filled metal–metal antibonding orbitals as there are metal–metal bonding ones [11b]. To summarize these observations, it appears that whenever the L ligand system has complete freedom of choice among the various coordination positions, the preferred structural type is **I** for d^1–d^1, and **II** for d^2–d^2, d^3–d^3, d^5–d^5 and d^6–d^6. There are no known d^4–d^4 ESBO compounds having the stoichiometry $M_2X_6L_4$ where L is a monodentate ligand.

Qualitative considerations led us to postulate that the π donating ability of the X ligands, especially when these are in axial positions, could be held responsible

for these peculiar structural changes. This has been an additional reason for us to re-examine the electronic structure of this family of ESBO compounds. We have used extended Huckel calculations to investigate the points we have raised above. This approximate molecular orbital method has been used a number of times before to adequately address questions of bonding and structure [1, 16] and it has proven to be useful again in this case.

Results and discussion

Importance of the reverse scissoring effect

As stated in 'Introduction', the size of the phosphine ligand may be invoked as a major contributing factor to the absence of an Mo–Mo bond in $Mo_2Cl_6(PEt_3)_4$ and the presence of a direct bond in $Mo_2Cl_6(PMe_2Ph)_4$ through the action of the steric interaction B (diagram **V**) and the 'reverse scissoring effect'. In order to find a theoretical basis for the effect of increasing phosphine bulk on the M–M separation in type **II** ESBO complexes we studied the model compounds $Mo_2Cl_6(PH_3)_4$ and *cis*-$[MoCl_4(PH_3)_2]^-$. In both cases, for different values of the angle subtended by the *cis* phosphine ligands and the Mo atom (α), the opposite angle (ϵ) was optimized (see **II** and **VI**). The results are tabulated in Table 1.

TABLE 1. (a) Variation of ϵ and Mo–Mo distance with α for $Mo_2Cl_6(PH_3)_4$, type **II**; (b) variation of ϵ with α for *cis*-$[MoCl_4(PH_3)_2]^-$ (**VI**)

α (°)	ϵ (°)	Mo–Mo (Å)
(a)		
70	84	3.547
75	83	3 575
80	83	3.575
85	82	3.603
90	81	3.631
95	81	3.631
100	80	3.658
105	79	3.686
110	79	3.686
115	78	3.713
(b)		
70	93	
75	92	
80	91	
85	89	
90	88	
95	87	
100	86	
105	85	
110	84	

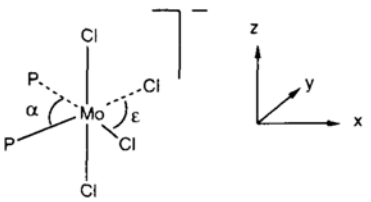

VI

Increasing α mimics the effect of increasing the steric bulk of the *cis* phosphine ligands. It is evident from the results shown in Table 1 that an increase in the angle α has the effect of pushing the *trans* Cl ligands closer together. The reason for this change can be traced to the rehybridization of the metal orbitals that are involved in the metal–ligand σ bonding with the four ligands in the equatorial plane. These hybrids can be seen to be composed of s, p_x, p_y and d_{xy} orbitals according to the choice of coordinates illustrated for **VI**. If $\alpha = \epsilon = 90°$, these four hybrids have equal contribution from the four atomic orbitals. If now α is decreased, the two hybrids involved in Mo–P bonding will increase their p_x contribution and decrease their p_y contribution, causing the opposite effect on the two hybrids involved in Mo–Cl binding. This will in turn cause an increase of the angle ϵ. The opposite effect will occur when α is increased, forcing ϵ to decrease. This 'reverse scissoring effect' can then be viewed as an electronic (rehybridization) effect which in this particular instance has its origin in a steric effect (the steric bulk of the two *cis* phosphine ligands). Our calculations show that the d-block orbitals (those originating from the t_{2g} set in ideal O_h symmetry) do not undergo drastic changes in energy during the molecular distortions.

Table 1 shows that the effect is less pronounced in **II** than in **VI**, i.e. ϵ changes by a smaller extent for a given change of α. This difference may be attributed to the coordination of the Cl atoms, *trans* to the phosphines, to another metal center which has in turn two *trans* chloro ligands. Our calculations were carried out by keeping invariant the geometry around the second metal, except for the angle ϕ which was allowed to vary in order to keep constant the Mo–Cl_{br} distances. It can be argued that the invariance of the angle β will tend to resist, through the reverse scissoring effect, a large variation of ϕ, therefore resisting a large variation of ϵ. Nevertheless, as Table 1(a) shows, an increase in α is predicted to result in a lengthening of the metal–metal bond. For obvious reasons, this lengthening is expected to occur to a larger degree for type **I** compounds.

Table 2 lists relevant structural parameters for selected type **I** and type **II** compounds. We have included only those series of compounds that have constant metal

TABLE 2 Selected geometric parameters for analogous type I and type II ESBO complexes

Compound	α (°)	ϵ (°)	ϕ (°)	β (°)	M–M (Å)	Ref.
Type I structure[a]						
$Zr_2Cl_6(dppe)_2$	76.25(9)	104 42(8)			3.099(2)	2b
$Zr_2Cl_6(PMe_2Ph)_4$	96.19(8)	104.26(8)			3.127(1)	2b
$Zr_2Cl_6(PEt_3)_4$	96.02(6)	102 81(5)			3.169(1)	2b
$Zr_2Cl_6(PBu_3)_4$	96.25(5)	102.57(5)			3 182(1)	2a
$Zr_2I_6(PMe_3)_4$	95.2(1)	107.96(5)			3.393(2)	2e
$Zr_2I_6(PMe_2Ph)_4$	94.75(4)	106.64(2)			3 4390(6)	2e
$Hf_2Cl_6(dippe)_2$	76 7(1)	104 0(1)			3 099(1)	2d
$Hf_2Cl_6(PMe_2Ph)_4$	96.02(5)	104.55(5)			3.0886(3)	2c
$Hf_2Cl_6(PEt_3)_4$	92.67(5)	104 62(5)			3 097(1)	2g
	98.95(6)	104.22(5)			3.118(1)	
$Hf_2I_6(PMe_2Ph)_6$	94.60(9)	107.03(3)			3.3948(6)	2e
Type II structure						
$W_2Cl_6(PMe_3)_4$	91 25(9)	110.01(8)	112.01(8)	86.10(9)	2.7113(8)	8e
$W_2Cl_6(PMe_2Ph)_4$	91.87(4)	109.75(4)	112.30(4)	86.47(4)	2 6950(3)	8d
$W_2Cl_6(PEt_3)_4$	92 48(8)	109 17(8)	111.35(8)	84.75(8)	2 7397(7)	8e
$Mo_2Cl_6(PMe_2Ph)_4$	96 83(5)	107 36(5)	109.69(5)	86 42(5)	2.8036(8)	6f
$Mo_2Cl_6(PEt_3)_4$	101 0(2)	82.7(1)	84.4(1)	93.4(2)	3 730(1)	6e

[a]For abbreviations see footnote a to Table 5

and donor atom sets, where variations in angular parameters can be more clearly analyzed in terms of the size of the L ligand. These are the d^1–d^1 (type **I**) $Zr_2Cl_6L_4$ and $Hf_2Cl_6L_4$ systems and the d^3–d^3 (type **II**) $W_2Cl_6L_4$ and $Mo_2Cl_6L_4$ systems where L is a tertiary phosphine in each series. The molybdenum complexes are those of greater relevance to this study. Unfortunately, there are no known examples of mononuclear *cis*-$[MX_4L_2]$ structures, all the known species with this stoichiometry having the *trans* stereochemistry. The data in Table 2 indicate that the type **I** systems of Zr(III) and Hf(III) are not so sensitive to changes in the steric hindrance of the phosphine ligands. For the zirconium system for instance, a comparison of entries 2–4 in the Table indicates that the value of α is practically insensitive to the steric bulk of the monodentate phosphine ligand, whereas comparison between the first entry and the following three indicates that an increase in α by 20° reduces the ϵ angle only by a couple of degrees, although this change is in the direction predicted by the reverse scissoring argument and this causes a significant lengthening of the Zr–Zr bond. The geometry of the $M_2(\mu\text{-}X)_2$ core in this system is obviously dominated by the metal–metal bond which, although formally only single (σ^2) [1], must be relatively strong notwithstanding the relatively long metal–metal separation. Further evidence for this is the reduction of α by more than one degree and the corresponding increase of ϵ on going from the chloro-bridged to the iodo-bridged complex. For the hafnium complexes, again, the value of α is little influenced by the nature of the phosphine ligands but it is interesting to note that two independent dimers were observed in the same crystal structure of $Hf_2Cl_6(PEt_3)_4$ [2g] and the change in the Hf–Hf distance reflects the change in α as predicted by our theoretical analysis. For the series of tungsten complexes, where the metal–metal bond is of type $\sigma^2\pi^2\delta^{*2}$, the trends in the values of α and ϵ are again consistent with the predicted steric effect. The corresponding variation of ϕ and β, however, does not clearly follow the trend predicted above and the M–M distance remains approximately constant, suggesting that these parameters might also be sensitive to other effects, perhaps even crystal packing effects. For the W_2^{6+} system, therefore, the strength of the metal–metal bond is still the dominating factor and the metal–metal distance is not greatly affected by the steric bulk of the equatorial phosphines through the reverse scissoring effect. It is to be noted, however, that for the $W_2Cl_6(dppe)_2$ complex which adopts the type **I** structure, the α angle is drastically reduced to 82.0(1)° and correspondingly ϵ opens up to 112.1(1)° allowing the metals to further approach each other at the level of 2.682(1) Å. Finally, for the pair of molybdenum compounds shown in Table 2, the changes are dramatic and fully reflect expectations based on the steric considerations above. Molybdenum(III) ESBO dimers with chelating ligands that adopt structural type **I** are always metal–metal bonded.

There are two additional ESBO systems that have been found to lack a metal–metal interaction when one is expected. One is the type **II** $Ru_2Cl_6L_4$ system ($L = PBu_3$, PEt_3) [10]. It would be interesting to synthesize a derivative with the smaller PMe_3 ligand or derivatives of type **I** with chelating ligands such as dppe to see whether these changes are sufficient to allow the metals to bind each other as is the case for Mo(III).

The other system is type **I** $Re_2Cl_6(dppe)_2$ [9a]. In this case, the equatorial dppe ligand has a small bite angle (α), which is a condition favoring the formation of a metal–metal interaction. It is therefore quite unlikely that, if an $Re_2Cl_6L_4$ compound with monodentate ligands will be made, this will exhibit a metal–metal bond. The type **III** $Ru_2Cl_6(dmpm)_2$ [4f] and $Re_2Cl_6(L\text{-}L)_2$ (L-L = $Me_2PCH_2PMe_2$, $Ph_2PCH_2PPh_2$) [4f, 8a] compounds most likely owe their metal–metal bonding interaction to the buttressing effect of the bidentate ligand. Furthermore, since metal–metal bonding is stronger for 5d than for 4d elements, it is also likely that metal–metal bonds will not be present in the yet unknown $Tc_2Cl_6L_4$ ESBO dimers in the absence of a buttressing effect.

Stability of ESBO structures with a d^0–d^0 configuration

We now wish to turn to the problem of the structural preference of ESBO complexes in a variety of d^n–d^n electronic configurations, viz. whether they exhibit or lack a metal–metal bonding interaction. We mentioned in 'Introduction' that a possible explanation for the difference in structural preference between type **I** and type **II** structures could reside in the M–X π interactions. In order to illustrate how this may come about, we first need to briefly summarize the known electronic structure of metal–metal bonded ESBO compounds [1]. The two pseudo-t_{2g} sets of metal orbitals (because of the particular choice of coordinates, these are the $d_{x^2-y^2}$, d_{xz} and d_{yz} orbitals) can interact with each other to give rise to three sets of metal–metal bonding and antibonding orbitals of σ, π and δ type (see Fig. 1). Qualitative overlap arguments would predict a $\sigma<\pi<\delta<\delta^*<\pi^*<\sigma^*$ relative ordering, but the involvement of X_{br} lone pairs through π bonding can modify this ordering by raising the energy of the π and δ orbital so that the latter ends up above the δ^*, and the ordering calculated in many cases [4f, 6b, f] is $\sigma<\pi<\delta^*<\delta<\pi^*<\sigma^*$. Besides X_{br}, also X_{ax} and X_{eq} possess lone pairs for π interaction with the d-block metal orbitals that are involved in metal–metal bonding. For our purposes, we shall only consider those X ligands that are double-sided π donors, i.e. having two mutually perpendicular π donor orbitals such as the halide ions. The terminal X ligands' lone pairs interact with the metal d-block orbitals to give rise to π bonding MOs which are mainly halogen-based and are located at lower energy in the MO diagram. The corresponding M–X π antibonding combinations end up in the mostly metal based metal–metal bonding and antibonding MOs of Fig. 1. Electronic occupation of these orbitals can therefore be expected to reduce the M–X π bonding. Our question is going to be whether a particular arrangement of the ligands will allow a more efficient M–X π bonding and whether this introduces a large enough energetic effect to justify the structural changes observed.

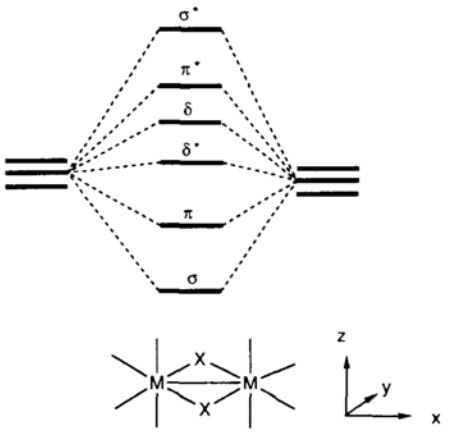

Fig. 1. Relative ordering of the d-block orbitals in a metal–metal bonded ESBO $M_2X_6L_4$ compound.

Because of the low local symmetry around each metal center, it is not possible to qualitatively partition the efficiency of the M–X π bonding interactions among the axial, equatorial and bridging X ligands. We recur then to the extended Huckel calculations, first asking the question: what is the situation for a dimer with no metal electrons (d^0–d^0 configuration) for type **I, II** and **III** structures? We have not considered structural type **IV** and others of lower symmetry for these calculations. The model compound used for this study was $[Mo_2Cl_6(PH_3)_3]^{6+}$ with the structural parameters obtained from the metal–metal bonded $Mo_2Cl_6(PMe_2Ph)_4$ structure [6f]. This is of course a completely unreal situation, not only because of the PH_3 substitution and the high positive charge on the complex, but also (and especially) because we are using a metal–metal separation typical of a metal–metal bonded complex whereas no metal–metal bond would exist for a d^0–d^0 complex. However, this calculation allows us to assess the structural preference in the absence of M–X π^* electrons and to obtain hypothetical bonding parameters for the M–X_{ax}, M–X_{eq} and M–X_{br} interactions against which to compare the corresponding parameters that will be calculated for the d^n–d^n configurations (see below). The results (see Table 3) indicate that structural type **I** is the most stable one, followed by type **II** and then type **III**, which is the least stable. As we have mentioned earlier, there are no known compounds of type **III** with monodentate ligands and our calculations indicate that indeed this structure is the least favored one. The geometry optimization also allows us to identify the *syn*–axial steric interaction (A in diagram **V**) as the probable responsible effect for the lower stability of **III**, since the value of the angles γ and δ increase as the steric interactions are alleviated on going from **III** to **I**. On the other hand, the *gem*–equatorial interaction (B in diagram **V**) does not appear to be as important

TABLE 3. Reduced overlap population (OP)[a] and energy data for $[Mo_2Cl_6(PH_3)_4]^{(6-2n)+}$ for d^n–d^n ($n = 0, 1, 2, 3$) configurations[b]

	Type I	Type II	Type III
d^0–d^0			
α (°)	80	81	
β (°)		84	85
γ (°)	166.5	163.5	
δ (°)		161	156
HOMO–LUMO gap (eV)	1.774	2.282	2.298
M–M OP	−0.013	0.010	0.010
$M–Cl_{ax}$ OP	0 554	0 551	
$M–Cl_{eq}$ OP		0.447	0.439
$M–Cl_{br}$ OP	0 498	0.516	0.513
Total energy (eV)	−1411.32	−1410.24	−1408.34
d^1–d^1			
HOMO–LUMO gap (eV)	0.908	0.614	0.295
M–M OP	0.152	0.160	0 175
$M–Cl_{ax}$ OP	0.554	0 551	
$M–Cl_{eq}$ OP		0.409	0 403
$M–Cl_{br}$ OP	0.480	0 497	0 494
Total energy (eV)	−1432.92	−1431 37	−1429.15
d^2–d^2			
HOMO–LUMO gap (eV)	0 183	0 032	0.033
M–M OP	0 289	0.273	0.149
$M–Cl_{ax}$ OP	0.508	0.526	
$M–Cl_{eq}$ OP		0.381	0.377
$M–Cl_{br}$ OP	0.439	0.448	0.494
Total energy (eV)	−1452.57	−1451.26	−1449.37
d^3–d^3			
HOMO–LUMO gap (eV)	0.397	0.611	0.595
M–M OP	0.263	0.250	0.285
$M–Cl_{ax}$ OP	0 449	0 486	
$M–Cl_{eq}$ OP		0.350	0.361
$M–Cl_{br}$ OP	0.439	0.443	0 440
Total energy (eV)	−1471.93	−1471 10	−1469.53
d^4–d^4			
HOMO–LUMO gap (eV)	0.141	0.026	0.002
M–M OP	0.289	0.273	0.310
$M–Cl_{ax}$ OP	0.407	0.423	
$M–Cl_{eq}$ OP		0.339	0.342
$M–Cl_{br}$ OP	0.380	0.381	0.371
Total energy (eV)	−1490.48	−1489.71	−1488.50
d^5–d^5			
HOMO–LUMO gap (eV)	0.912	1.122	1.312
M–M OP	0.128	0.123	0.126
$M–Cl_{ax}$ OP	0.345	0.341	
$M–Cl_{eq}$ OP		0.330	0.328
$M–Cl_{br}$ OP	0.380	0.379	0.371
Total energy (eV)	−1508.76	−1508.27	−1507.46

[a]Overlap populations are the calculated Mulliken overlap populations, $2c_ic_jS_{ij}$. [b]Structures are optimized in the d^0–d^0 configuration.

for this model system, since the α angle (P_{eq}–M–P_{eq}) is not greatly different, in fact it is even smaller, than the β angle (Cl_{eq}–M–Cl_{eq}).

What happens now when these ideas are translated into the real systems having much larger L ligands than the PH_3 model ligand used for our calculations? Let us remember that mononuclear compounds with the MX_4L_2 stoichiometry prefer to adopt the *trans* geometry. The probable reason for this choice is the less favorable steric interaction that exists in the *cis* isomer between the two bulky L ligands (analogous to B in diagram **V**). It can also be noted that the angle α in type **I** and **II** ESBO dimers (where B interactions exist) is usually much greater than the value obtained from our energy minimization (e.g. see structural data in Table 2). From the point of view of the individual metal centers in the ESBO dimers, the L ligands should therefore prefer to occupy an axial site to avoid the B interaction. However, by doing so on both metals they introduce the unfavorable A repulsion. A compromise is found in structure **II**. Thus, these simple steric considerations allow a rationale for the preference of structural type **II** in most cases. By a natural extension of these ideas, it is also possible to predict that a reduction in the steric bulk of the ligand L and a lengthening of the M–M separation (e.g. compounds without a metal–metal bond) may allow the existence of structure **III** for complexes with monodentate ligands.

An analysis of the overlap populations (OP) of each type of M–X bond (Table 3, d^0–d^0 system) places them in the order $M–Cl_{eq} < M–Cl_{br} < M–Cl_{ax}$. This trend parallels the trend of Mo–Cl bond distances that were used for the calculations (the greater overlap population corresponding to the shorter bond length), which were obtained from the X-ray structure of the metal–metal bonded d^3–d^3 $Mo_2Cl_6(PMe_2Ph)_4$ complex. These numbers have no meaning by themselves but serve as terms of comparison for the corresponding calculated numbers for d^n–d^n dimers ($n < 0$), see next section.

Structural preference for d^n–d^n ESBO complexes ($n \leqslant 0$)

It is now interesting to analyze the expected changes upon introduction of electrons into the metal–metal bonding orbitals. These orbitals are illustrated for structural types **I** and **II** in Figs. 2 and 3, respectively. It is straightforward to see that the lone pairs of axial X ligands interact quite strongly with the π, π^*, δ and δ^* MOs, but they do not interact at all with the σ and σ^* orbitals. The corresponding lone pairs of the equatorial X ligands, on the other hand, interact with all the metal–metal bonding and antibonding combinations, but the strongest interaction is with the σ and σ^* combinations. The π, π^*, δ and δ^* combinations show a reduced overlap with the X_{eq} lone pairs because of the 45° offset between the planes of maximum electron density of the X and M orbitals and it is therefore expected that the presence of electrons in these four orbitals contributes less to the destabilization of the M–X π bond. Thus, it is easy to predict that the introduction of two electrons (d^1–d^1) to achieve a single

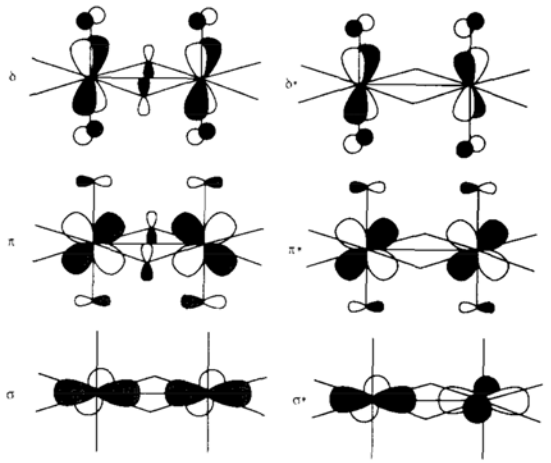

Fig. 2. Qualitative picture of the d-block MOs for a metal–metal bonded ESBO complex of type **I**.

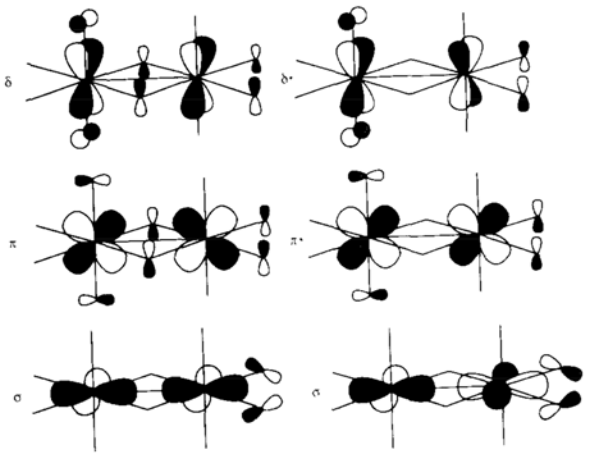

Fig. 3. Qualitative picture of the d-block MOs for a metal–metal bonded ESBO complex of type **II**.

metal–metal bond (σ^2) will destabilize the type **II** structure but not **I**. Introduction of additional electrons up to d^5–d^5 should on the other hand, destabilize structure **I** to a greater extent than structure **II**.

These ideas find numerical support in our calculations. Table 3 shows the variation of bonding parameters for the series of complexes $[Mo_2Cl_6(PH_3)_4]^{(6-2n)+}$ for the d^n–d^n dimers of types **I**, **II** and **III**. The molecular geometries were maintained fixed and identical to those of minimum energy for the d^0–d^0 structures. The most relevant results are as follows. (i) The structural type **I** is always calculated as the energetically most favorable one. However, the energy difference between **I** and **II** increases on going from d^0–d^0 to d^1–d^1, then it decreases again. This trend is shown in Fig. 4. (ii) The Mo–Mo overlap population for both **I** and **II** is practically zero for d^0–d^0 and follows the trend d^1–d^1 < d^2–d^2 > d^3–d^3 < d^4–d^4 > d^5–d^5, as expected for the successive occupation of the σ, π, δ^*, δ and π^* orbitals;

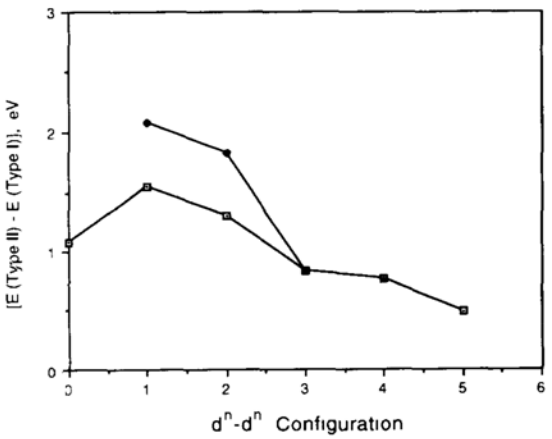

Fig. 4. Calculated energy difference between structures **I** and **II** as a function of d^n–d^n electronic configuration. –□– $[Mo_2Cl_6(PH_3)_4]^{(6-2n)+}$, –◆– $M_2Cl_6(PH_3)_4$ (M = Zr, Nb, Mo).

on the other hand, the trend of the Mo–Mo OP is different for **III** and is in line with the relative orbital ordering $\sigma < \delta^* < \pi < \delta < \pi^* < \sigma^*$ in this case. (iii) The changes in OP for any particular type of Mo–Cl bond on going from one structural type to another within the same d^n–d^n configuration are small relative to the changes observed upon changing the d-electron count within the same structural type, and are as expected on the basis of our qualitative model. For instance, the Mo–Cl_{ax} OP in both **I** and **II** remains the same on going from d^0–d^0 to d^1–d^1, whereas at the same time the Mo–Cl_{eq} OP in **II** and **III** decreases. On the other hand, on going from d^1–d^1 to d^2–d^2 and for each subsequent step until d^5–d^5, the Mo–Cl_{eq} OP continues to slightly decrease but now the Mo–Cl_{ax} OP experiences an even greater decrease. (iv) The Mo–Cl_{br} OP decreases the most as a result of the occupation of the metal–metal π and δ orbitals, whereas it remains constant upon occupation of the metal–metal δ^* and π^* orbitals. This trend is also fully consistent with our qualitative model. The trends in Mo–Cl OP will be later compared with actual published M–Cl bond distances after we have concluded our analysis on the structural choice.

A possible problem with these calculations in the extrapolation to real systems as far as the relative total energy of the various structural types goes is that the geometry of the molecule and all bond distances were kept fixed at the values optimized for the d^0–d^0 structure. We have carried out additional calculations for the analogous series of models $M_2Cl_6(PH_3)_4$ (M = Zr, d^1–d^1; Nb, d^2–d^2; Mo, d^3–d^3) by using bond lengths from known X-ray structures and by optimizing the bond angles α, γ, δ and β to attain a minimum energy. The relevant results are shown in Table 4. All the trends discussed earlier for the data in Table 3 are the same here, except that we observe greater variations in OP upon

TABLE 4. Reduced overlap population (OP)[a] and energy data for Zr, Nb and Mo ESBO models

	Type I	Type II
$Zr_2Cl_6(PH_3)_4$, d^1–d^1		
HOMO–LUMO gap (eV)	1.712	0.732
M–M OP	0.176	0.192
M–Cl_{ax} OP	0.792	0.788
M–Cl_{eq} OP		0.660
M–Cl_{br} OP	0.555	0 558
Total energy (eV)	−1449.28	−1447.20
$Nb_2Cl_6(PH_3)_4$, d^2–d^2		
HOMO–LUMO gap (eV)	0.475	0.207
M–M OP	0.406	0.415
M–Cl_{ax} OP	0.664	0.689
M–Cl_{eq} OP		0.493
M–Cl_{br} OP	0.523	0.530
Total energy (eV)	−1473.78	−1471.95
$Mo_2Cl_6(PH_3)_4$, d^3–d^3		
HOMO–LUMO gap (eV)	0 391	0 614
M–M OP	0.259	0.248
M–Cl_{ax} OP	0 452	0.486
M–Cl_{eq} OP		0.351
M–Cl_{br} OP	0.438	0.443
Total energy (eV)	−1471.95	−1471.11

[a]Overlap populations reported are the calculated Mulliken overlap populations, $2c_ic_jS_{ij}$.

change of electronic configuration, which reflects the change in the nature of the metal center.

The difference between the total energy of structures **I** and **II** as a function of the d^n–d^n configuration for the series of models of Tables 3 and 4 is illustrated in Fig. 4. Although the calculations predict a more stable type **I** structure for all electronic configurations, it is reasonable to expect that when PH_3 is replaced by a more bulky L ligand, the energy difference will be reduced because there are two unfavorable B interactions in structure **I** as compared with only one in structure **II**. It is therefore natural to postulate that the unfavorable steric effect of type B is worth a sufficient amount of energy to make structure **II** more favorable for the electronic configurations d^2–d^2 and above, whereas for d^1–d^1 the electronic effect is stronger and will drive the structure to type **I**. The results of these calculations are consistent with the M–X π interaction as being responsible for this electronic effect.

Trends in the M–X bond lengths

Other interesting trends from the results of the calculations of type **I** and type **II** ESBO dimers shown in Tables 3 and 4 are the following: (i) for each d^n–d^n configuration, the M–Cl_{ax} OP is greater than the M–Cl_{eq} OP; (ii) the M–Cl_{br} OP is always smaller than the M–Cl_{ax} OP except for the d^5–d^5 configuration, but is usually greater than the M–Cl_{eq} OP, the only exception being the type **II** d^1–d^1 $Zr_2Cl_6(PH_3)_4$ model which does not have experimental counterparts. These findings and the trends in the M–Cl OP as a function of d^n–d^n configuration that have been discussed earlier are in very good agreement with trends observed for the M–X_{ax}, M–X_{eq} and M–X_{br} distances in known type **I**, **II** and **III** structures, which are collected in Table 5. First, we observe that for M–M non-bonded compounds, also reported in Table 5, the M–X_{ax} and M–X_{eq} distances are statistically equivalent in most cases, and that the M–X_{br} are always longer, as is normal to expect because the X_{br} ligand is shared between two metal centers. Also evident is the *trans* influence in type **II** structures, which is responsible for the M–X_{br} bonds *trans* to P donors being significantly longer than the M–X_{br} bonds *trans* to X. Finally, the expected decrease of the lengths upon going from left to right of the transition series, due to the metal contraction, is observed. For M–M bonded compounds, however, the situation changes substantially and the following points are observed. (i) The M–X_{ax} bonds are *always* significantly shorter than the M–X_{eq} bonds. This is true whether bonds within the same molecule (e.g. type **II**) are directly compared, or a comparison is made between bonds in different molecules of types **I**, **II** and **III** as long as the nature of M, X and the d^n–d^n count are kept the same. (ii) Whereas a *trans* influence on the M–X_{br} bonds is still observed as in the non-bonded structures, the M–X_{br} bonds in metal–metal bonded structures are *always* either significantly shorter than, or at most statistically equivalent to the M–X_{eq} bonds (cf. with the non-bonded compounds, where M–X_{br} bonds are always significantly longer than M–X_{eq} bonds). In all of the reported type **II** d^3–d^3 structures, the M–X_{br} bonds (*trans* to X) are even shorter than the M–X_{ax} bonds.

All-compound averages for the M–Cl_{ax}, M–Cl_{eq} and M–Cl_{br} bond lengths as a function of d^n–d^n configuration are tabulated in Table 6 and illustrated in Fig. 5. Since the calculations show comparable OPs for the same bonds in different structural types, we feel confident in averaging the experimental bond lengths from different structural types, that is, the average M–Cl_{ax} distances are obtained from both types **I** and **II**, M–Cl_{eq} from both types **II** and **III**, and M–Cl_{br} (*trans* to Cl) both from types **II** and **III**. The trends shown in Fig. 5 are particularly enlightening. A general M–Cl bond shortening on going from $n=1$ to $n=5$ is expected because of the metal contraction along this series. This decrease is most evident for the M–Cl_{eq} distances. As discussed above, filling up the π, δ, δ^* and π^* orbitals does not largely affect the strength of the M–Cl_{eq} π interaction, thus the observed decrease in M–Cl_{eq} distances as a function of d^n–d^n configuration should closely reflect the decrease expected on the basis of metal radius considerations. The M–Cl_{ax} π interaction, on the other hand, is more substantially reduced by oc-

TABLE 5. Comparison of $M-X_{ax}$, $M-X_{eq}$ and $M-X_{br}$ distances for $M_2X_6L_4$ complexes

Formula[a]	$M-Cl_{ax}$	$M-Cl_{eq}$	$M-Cl_{br}$[a]	Type	d^n-d^n	Ref
M–M bonded dimers						
$Zr_2Cl_6(PBu_3)_4$	2 431(2)		2.544(2)	I	d^1-d^1	2a
$Zr_2Cl_6(PEt_3)_4$	2.424(6)		2.540(2)	I	d^1-d^1	2b
$Zr_2Cl_6(PMe_2Ph)_4$	2.417(12)		2.547(12)	I	d^1-d^1	2b
$Zr_2Cl_6(dppe)_2$	2.420(3)		2.537(8)	I	d^1-d^1	2b
$Zr_2I_6(PMe_3)_4$	2.805(2)		2.885(4)	I	d^1-d^1	2e
$Zr_2I_6(PMe_2Ph)_4$	2.799(19)		2.878(5)	I	d^1-d^1	2e
$Hf_2Cl_6(PMe_2Ph)_4$	2.412(2)		2.524(6)	I	d^1-d^1	2c
$Hf_2Cl_6(dippe)_2$	2 408(4)		2.517(4)	I	d^1-d^1	2d
$Hf_2Cl_6(PEt_3)_4$	2.417(2)		2.532(2)	I	d^1-d^1	2g
	2.415(2)		2.538(2)			
$Hf_2I_6(PMe_2Ph)_4$	2.779(19)		2 855(2)	I	d^1-d^1	2e
$Nb_2Cl_6(dppm)_2$	2.400(2)		2 454(13)	I	d^2-d^2	4c
$Nb_2Cl_6(dppe)_2$	2.397(6)		2.450(12)	I	d^2-d^2	4d
$Nb_2Cl_6(depe)_2$	2.410(13)		2.451(19)	I	d^2-d^2	4g
$Ta_2Cl_6(depe)_2$	2.408(13)		2.442(8)	I	d^2-d^2	4h
$Ta_2Cl_6(dmpe)_2$	2.415(7)		2.460(1)	I	d^2-d^2	4b
$Ta_2Cl_6(PMe_3)_4$	2.399(3)	2.480(7)	2.473(4), 2.430(3)	II	d^2-d^2	4a
$Ta_2Cl_6py_4$	2.400(6)	2.458(13)	2.420(3), 2.452(6)	II	d^2-d^2	4i
$Nb_2Cl_6(dmpm)_2$		2.444(5)	2.438(6)	III	d^2-d^2	4e
$Ta_2Cl_6(dmpm)_2$		2.446(11)	2.433(6)	III	d^2-d^2	4f
$Mo_2Cl_6(dppe)_2$	2.394(3)		2.413(6)	I	d^3-d^3	6c, h
$Mo_2Cl_6(dedppe)_2$	2.403(7)		2.424(5)	I	d^3-d^3	6c
$W_2Cl_6(dppe)_2$	2.394(6)		2.402(3)	I	d^3-d^3	6c
$Mo_2Cl_6(PMe_2Ph)_4$	2.398(3)	2.441(3)	2 418(2), 2.383(3)	II	d^3-d^3	6f
$W_2Cl_6(PMe_3)_4$	2.413(2)	2.462(5)	2 408(2), 2 380(8)	II	d^3-d^3	8e
$W_2Cl_6(PMe_2Ph)_4$	2.399(1)	2.454(1)	2 398(1), 2.361(1)	II	d^3-d^3	8d
$W_2Cl_6(PEt_3)_4$	2.407(5)	2.452(2)	2.412(2), 2.380(4)	II	d^3-d^3	8e
$W_2Cl_6py_4$	2.397(8)	2.430(8)	2.392(8), 2.392(7)	II	d^3-d^3	8a
$Mo_2Cl_6(dmpm)_2$		2.428(2)	2.390(3)	III	d^3-d^3	8a
$Mo_2Cl_6(dppm)_2$		2.396(4)	2.403(2)	III	d^3-d^3	4f
$Mo_2Br_6(dppm)_2$		2.553(13)	2.516(7)	III	d^3-d^3	6d
$Mo_2I_6(dppm)_2$		2.791(2)	2.698(7)	III	d^3-d^3	6d
$W_2Cl_6(dmpm)_2$		2.439(2)	2.385(2)	III	d^3-d^3	8a
$W_2Cl_6(dppm)_2$		2.410(2)	2.399(6)	III	d^3-d^3	8a
$[Re_2Cl_6(dppm)_2]^+$		2.356(4)	2.356(7)	III	d^3-d^4	9d
$Re_2Cl_6(dmpm)_2$		2.408(2)	2.369(1)	III	d^4-d^4	8a
$Re_2Cl_6(dppm)_2$		2.388(3)	2.390(2)	III	d^4-d^4	4f
$Ru_2Cl_6(dmpm)_2$		2 353(2)	2.344(10)	III	d^5-d^5	4f
Non-bonded dimers						
$Cr_2Cl_6(PMe_3)_4$	2.286(5)	2.286(9)	2.398(5), 2.391(5)	II	d^3-d^3	5
$Cr_2Cl_6(PEt_3)_4$	2.289(2)	2.284(3)	2.423(4), 2.388(6)	II	d^3-d^3	5
$Cr_2Cl_6(dmpm)_2$		2.277(1)	2.380(1)	III	d^3-d^3	5
$Mo_2Cl_6(PEt_3)_4$	2.384(3)	2.376(5)	2.521(4), 2.480(4)	II	d^3-d^3	6e
$Re_2Cl_6(dppe)_2$	2.314(8)		2 499(3)	I	d^4-d^4	9a
$Ru_2Cl_6(PBu_3)_4$	2.331(2)	2.324(3)	2.504(3), 2.414(3)	II	d^5-d^5	10a
$Rh_2Cl_6(PBu_3)_4$	2.321(12)	2.346(14)	2.523(16), 2 394(13)	II	d^6-d^6	11a
$Rh_2Cl_6(dppm)_2$		2.308(3)	2.372(3)	III	d^6-d^6	11b
$Rh_2Br_6(dppm)_2$		2.452(5)	2.490(4)	III	d^6-d^6	11b

[a]Abbreviations used are as follows: dppe = 1,2-bis(diphenylphosphino)ethane; dippe = 1,2-bis(diisopropylphosphino)ethane; dppm = 1,2-bis(diphenylphosphino)methane; depe = 1,2-bis(diethylphosphino)ethane; dmpe = 1,2-bis(dimethylphosphino)ethane; dmpm = 1,2-bis(dimethylphosphino)methane; dedppe = 1-diethylphosphino-2-diphenylphosphinoethane. [b]For type **II** structures, the first value is the distance to the metal that holds the X_{ax} ligands, the second value is the distance to the metal that holds the X_{eq} ligands.

cupation of the π, δ, δ^* and π^* orbitals. In agreement with this, the $M-X_{ax}$ distance decreases by a much lesser extent on going from d^1-d^1 to d^3-d^3 than does the $M-Cl_{eq}$ distance. Our considerations allow the prediction of a small decrease in $M-Cl_{ax}$ upon going further to d^4-d^4 and d^5-d^5. Extrapolation of the $M-Cl_{ax}$ curves in Fig. 5 to the d^5-d^5 configuration indicates that this distance should become longer than the $M-Cl_{eq}$ distance in agreement with the calculated smaller $Mo-Cl_{ax}$ OP with respect to the $Mo-Cl_{eq}$ OP in the d^5-d^5

TABLE 6. Averages of M–Cl_{ax}, M–Cl_{eq} and M–Cl_{br} (*trans* to Cl) distances for the $M_2Cl_6L_4$ complexes of types **I**, **II** and **III** reported in Table 5

	M–Cl_{ax}		M–Cl_{eq}		M–Cl_{br}	
	4d	5d	4d	5d	4d	5d
d^1–d^1	2.423(6)	2.413(3)				
d^2–d^2	2.402(7)	2.405(8)	2.444(5)	2.461(17)	2.438(6)	2 438(12)
d^3–d^3	2.398(5)	2.402(8)	2.422(23)	2 441(19)	2.392(10)	2 383(13)
d^4–d^4				2.398(10)		2.380(11)
d^5–d^5			2.353(2)		2.344(10)	

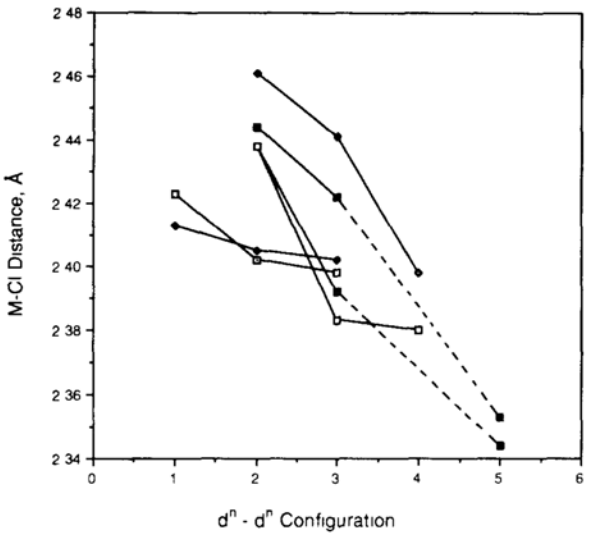

Fig. 5. Variation of experimental M–Cl distances (see Table 6) as a function of d^n–d^n electronic configuration. –□– M–Cl_{ax}, 4d; –◆– M–Cl_{ax}, 5d; –■– M–Cl_{eq}, 4d; –◇– M–Cl_{eq}, 5d, –■– M–Cl_{br}, 4d, –□– M–Cl_{br}, 5d.

$[Mo_2Cl_6(PH_3)]^{4-}$ model. To test for this, it would be interesting to obtain a metal–metal bonded structure for a type **I** or type **II** $Ru_2Cl_6L_4$ compound. Finally, concerning the experimental M–Cl_{br} distances, we observe the marked decrease on going from d^2–d^2 to d^3–d^3, corresponding to the occupation of the δ^* orbital which has no symmetry allowed M–Cl_{br} π interaction. Although data are not available for ESBO $M_2Cl_6L_4$ complexes of d^4 Tc(III) and d^5 Os(III), the data available so far seem to suggest that the M–Cl_{br} bond shortening is not pronounced on going from d^3–d^3 to d^4–d^4, whereas a greater shortening is observed again on going further to d^5–d^5. This trend is in perfect agreement with the orbital ordering shown in Fig. 1, which places the δ^* orbital below the δ orbital. More importantly, this trend and all the trends analyzed here confirm that M–X π interactions play a significant role in the bonding for this class of molecules and thus presumably also in their thermodynamic stability.

Conclusions

The present study has shown that the interplay of steric effects, metal–metal bonding and metal–ligand bonding in ESBO compounds with the $M_2X_6L_4$ stoichiometry is more complex and interesting than previously appreciated. In particular, two different questions pertaining to the structure and stability of this class of molecules have been addressed. The first one is related to the ability of Mo(III) to establish metal–metal bonding interactions. As we have discussed earlier [6e, f], while the metal–metal non-bonded structure (favored by high pairing energies) is preferred by Cr(III) dimers and the metal–metal bonded structure (favored by strong metal–metal overlap) is preferred by W(III) dimers, there is a very delicate balance between the two stabilizing factors in the corresponding compounds of Mo(III). It is therefore possible and, on the basis of the calculations presented here, quite likely, that the difference in steric bulk between PMe_2Ph and PEt_3 is sufficient to tip the balance in either direction.

The second point is the preference of $M_2X_6L_4$ compounds with monodentate L ligands for a type **I** structure when the configuration is d^1–d^1 and for a type **II** structure for any other configuration either with or without a metal–metal bond. A simple rationalization for this phenomenon has been provided which is based on a combination of steric (A and B interactions) and electronic (M–X π interactions) effects. The calculations that we have carried out also allow us to rationalize unusual trends in the experimental M–X bond lengths as M is changed across the transition series.

Experimental

Extended Huckel calculations [17] were carried out with a weighted H_{ij} formula [18]. A modified version was used for molecular orbital analysis [19]. The parameters taken from previous calculations [16, 20] are listed in Table 7.

The ESBO model compounds have idealized D_{2h} (type **I** and type **III**) or C_{2v} (type **II**) symmetry and

TABLE 7. Extended Huckel parameters

Atom	Orbital	H_{ii}	Orbital exponent[a]	
			1	2
Zr	5s	−9.87	1.817	
	5p	−6.76	1.776	
	4d	−11.18	3.835	1.505
			(0.6230)	(0.5787)
Nb	5s	−10.10	1.89	
	5p	−6.86	1.85	
	4d	−12.10	4.08	1.64
			(0.6401)	(0.5516)
Mo	5s	−8.34	1.96	
	5p	−5.24	1.92	
	4d	−10 50	4.54	1.90
			(0.5899)	(0.5899)
Cl	3s	−26 3	2.183	
	3p	−14.2	1 733	
P	3s	−18.6	1.60	
	3p	−14.0	1.60	
H	1s	−13.6	1 30	

[a]Values in parentheses are the coefficients in the double ζ expansion of the d orbitals.

are based on reported structural data. All M–P–H angles and H–P–H angles were taken as 109.5°. Other geometric parameters are given below. For the *cis*-$[MoCl_4(PH_3)_2]^-$, the appropriate cut from the ESBO model was used.

$Mo_2Cl_6(PH_3)_4$ (all types). Mo–Mo = 2.804; Mo–Cl_{ax} = 2.398; Mo–Cl_{eq} = 2.441; when *trans* to an Mo–P bond, Mo–Cl_{br} = 2.418; when *trans* to an Mo–Cl bond, Mo–Cl_{br} = 2.383; Mo–P_{ac} = 2.576; Mo–P_{eq} = 2.583 Å.

$Nb_2Cl_6(PH_3)_4$ (types I and II). All Nb–ligand distances were averages of those for known $Nb_2Cl_6L_4$ complexes. Nb–Nb = 2.721; Nb–Cl_{ax} = 2.402; Nb–Cl_{eq} = 2.444; when *trans* to an Nb–P bond, Nb–Cl_{br} = 2.451; when *trans* to an Nb–Cl bond, Nb–Cl_{br} = 2.438; Nb–P_{ax} = 2.630; Nb–P_{eq} = 2.659 Å.

$Zr_2Cl_6(PH_3)_4$ (types I and II). Zr–Zr = 3.127; Zr–Cl_{ax} = 2.417; Zr–Cl_{eq} = 2.417; Zr–Cl_{br} = 2.547; Zr–P_{ax} = 2.765; Zr–P_{eq} = 2.765 Å.

Acknowledgements

Support from the National Science Foundation (CHE-9058375), the Exxon Education Foundation and the Alfred P. Sloan Foundation are gratefully acknowledged. We are also indebted to Professors F.A. Cotton, M.H Chisholm and G.G. Stanley for helpful discussions and for keeping us informed of their unpublished work.

References

1 S. Shaik, R. Hoffmann, C R. Fisel and R.H. Summerville, *J. Am. Chem Soc*, *102* (1980) 4555.
2 (a) J.H. Wengrovius, R.R. Schrock and C.S Day, *Inorg Chem*, *20* (1981) 1844, (b) F.A. Cotton, M.P Diebold and P.A. Kibala, *Inorg Chem*, *27* (1988) 799; (c) F.A. Cotton, P.A. Kibala and W.A. Wojtczak, *Inorg Chim. Acta, 177* (1990) 1; (d) P.M. Morse, S.R. Wilson and G.S. Girolami, *Inorg. Chem., 29* (1990) 3200, (e) F.A Cotton, M. Shang and W.A. Wojtczak, *Inorg. Chem*, *30* (1991) 3670; (f) D.M. Hoffman and S. Lee, *Inorg Chem., 31* (1992) 2676; (g) M.E. Riehl, S.R. Wilson and G.S. Girolami, *Inorg Chem., 32* (1993) 218.
3 (a) A.J. Benton, M.G.B. Drew, R.J. Hobson and D. Rice, *J. Chem. Soc, Dalton Trans.*, (1981) 1304; (b) M.G.B. Drew, D.A. Rice and D.M. Williams, *J Chem. Soc, Dalton Trans.*, (1985) 417; (c) E. Babaian-Kibala, F.A. Cotton and P.A. Kibala, *Inorg. Chem., 29* (1990) 4002; (d) E. Babaian-Kibala and F.A. Cotton, *Inorg. Chim Acta, 182* (1991) 77.
4 (a) A.P Sattelberger, R.B. Wilson, Jr. and J.C. Huffman, *Inorg Chem*, *21* (1982) 2393; (b) F.A. Cotton, L.R. Falvello and R.C. Najjar, *Inorg. Chem*, *22* (1983) 375; (c) F.A. Cotton and W.J. Roth, *Inorg. Chem*, *22* (1983) 3654; (d) *Inorg Chim Acta, 71* (1983) 175; (e) F.A. Cotton, S.A. Duraj, L.R. Falvello and W.J. Roth, *Inorg. Chem., 24* (1985) 4389, (f) A.R. Chakravarty, F A. Cotton, M.P. Diebold, D.B. Lewis and W.J. Roth, *J. Am Chem Soc*, *108* (1986) 971; (g) J.M. Canich and F.A. Cotton, *Inorg. Chem., 26* (1987) 4236; (h) F.A. Cotton, M.P. Diebold and W.J. Roth, *Inorg. Chem*, *26* (1987) 4130; (i) E. Babaian-Kibala and F A. Cotton, *Inorg. Chim Acta, 171* (1990) 71.
5 F A. Cotton, J.L. Eglin, R.L. Luck and K. Son, *Inorg Chem*, *29* (1990) 1802.
6 (a) F.A. Cotton, P.E. Fanwick and J.W. Fitch III, *Inorg. Chem., 17* (1978) 3254; (b) F.A. Cotton, M.P. Diebold, C.J. O'Connor and G.L. Powell, *J Am. Chem Soc*, *107* (1985) 7438; (c) P.A. Agaskar, F A. Cotton, K.R. Dunbar, L.R. Falvello and C.J. O'Connor, *Inorg Chem., 26* (1987) 4051; (d) F.A. Cotton, L.M. Daniels, K.R. Dunbar, L R. Falvello, C.J. O'Connor and A.C. Price, *Inorg. Chem*, *30* (1991) 2509; (e) H.D. Mui and R. Poli, *Inorg. Chem., 28* (1989) 3609; (f) R. Poli and H.D. Mui, *Inorg Chem., 30* (1991) 65, (g) R. Poli and J.C Gordon, *J Am Chem. Soc., 114* (1992) 6723; (h) R. Poli and B.E. Owens, *Gazz. Chim. Ital, 121* (1991) 413.
7 (a) F.A. Cotton, C.A. James and R.L. Luck, *Inorg Chem., 30* (1991) 4370; (b) F.A. Cotton, J.L. Eglin, C.A. James and R.L. Luck, *Inorg Chem., 31* (1992) 5308.
8 (a) R.B. Jackson and W.E Streib, *Inorg Chem, 10* (1971) 1760; (b) J.A.M. Canich, F.A. Cotton, L.M. Daniels and D.B. Lewis, *Inorg Chem*, *26* (1987) 4046; (c) S.T. Chacon, M.H. Chisholm, W.E. Streib and W.G. Van Der Sluys, *Inorg Chem*, *28* (1992) 6; (d) F.A. Cotton and S.K. Mandal, *Inorg Chem., 31* (1992) 1267; (e) J.T. Barry, S.T Chacon, M.H. Chisholm, V.F. DiStasi, J.C. Huffman, W.E. Streib and W.G. Van Der Sluys, *Inorg. Chem., 32* (1993) 2322.
9 (a) J.A. Jaecker, W.R Robinson and R.A. Walton, *J. Chem Soc., Dalton Trans*, (1975) 698; (b) T.J. Barder, F.A. Cotton, D. Lewis, W. Schwotzer, S.M. Tetrick and R.A. Walton, *J. Am Chem Soc*, *106* (1984) 2882; (c) B.J. Heyen and G.L. Powell, *Inorg Chem., 29* (1990) 4574; (d) K.R. Dunbar, D. Powell and R.A. Walton, *Inorg Chem., 24* (1985) 2842.
10 (a) F.A. Cotton, M. Matusz and R.C. Torralba, *Inorg Chem*, *28* (1989) 1516; (b) F A Cotton and R.C. Torralba, *Inorg Chem., 30* (1991) 4392

11 (a) J.A Muir, M M. Muir and A.J. Rivera, *Acta Crystallogr., Sect B, 30* (1974) 2062; (b) F.A. Cotton, K.R Dunbar, C.T. Eagle, L.R. Falvello and A.C. Price, *Inorg Chem, 28* (1989) 1754; (c) F A. Cotton, J.L. Eglin and S.-J Kang, *J Am Chem Soc, 114* (1992) 4015.
12 F.A. Cotton, *Polyhedron, 6* (1987) 667.
13 K.J. Ahmed, J.C Gordon, H D. Mui and R. Poli, *Polyhedron, 10* (1991) 1667
15 R. Poli, *Comments Inorg Chem, 12* (1992) 285.
16 (a) R H. Summerville and R. Hoffmann, *J Am. Chem Soc, 98* (1976) 7240; (b) *101* (1979) 3821.
17 (a) R Hoffmann, *J. Chem Phys, 39* (1963) 1397, (b) R. Hoffmann and W.N. Lipscomb, *J Chem Phys, 36* (1962) 3179; (c) *37* (1962) 2872
18 J.H. Ammeter, H.B Burgi, J.C. Thibeault and R. Hoffmann, *J Am. Chem. Soc, 101* (1978) 3686.
19 C. Mealli and D. Proserpio, *J Chem Educ, 67* (1990) 399.
20 K. Tatsumi, A Nakamura, P. Hofmann, P Stauffert and R. Hoffmann, *J Am Chem Soc, 107* (1985) 4440